
AlignFlow: Cycle Consistent Learning from Multiple Domains via Normalizing Flows

Aditya Grover*, Christopher Chute*, Rui Shu, Zhangjie Cao, Stefano Ermon
Computer Science Department
Stanford University
{adityag, chute, ruishu, caozj, ermon}@cs.stanford.edu

Abstract

Given unpaired data from multiple domains, a key challenge is to efficiently exploit these data sources for modeling a target domain. Variants of this problem have been studied in many contexts, such as cross-domain translation and domain adaptation. We propose AlignFlow, a generative modeling framework for learning from multiple domains via normalizing flows. The use of normalizing flows in AlignFlow allows for a) flexibility in specifying learning objectives via adversarial training, maximum likelihood estimation, or a hybrid of the two methods; and b) exact inference of the shared latent factors across domains at test time. We derive theoretical results for the conditions under which AlignFlow guarantees marginal consistency for the different learning objectives. Furthermore, we show that AlignFlow guarantees *exact* cycle consistency in mapping datapoints from one domain to another. Empirically, AlignFlow can be used for data-efficient density estimation given multiple data sources and shows significant improvements over relevant baselines on unsupervised domain adaptation.

1 Introduction

In recent years, there has been an increase in the availability of both labeled and unlabeled datasets from multiple sources. For example, many variants of face datasets scraped from sources such as Wikipedia and IMDB are publicly available. Given data from two or more domains, we expect sample-efficient learning algorithms to be able to learn and *align* the shared structure across these domains for accurate downstream tasks. This perspective has a broad range of applications across machine learning, including relational learning [1], domain adaptation [2–4], image and video translation for computer vision [5, 6], and machine translation [7], especially for low resource languages [8].

Many variants of the domain alignment problem have been studied in prior work. For instance, *unpaired cross-domain translation* refers to the task of learning a mapping from one domain to another given datasets from the two domains [9]. This task can be used as a subproblem in the *domain adaptation* setting, where the goal is to learn a classifier for the unlabeled domain given labeled data from a related source domain [10]. Many of these problems are underconstrained due to the limited supervision available and an amalgam of inductive biases need to be explicitly enforced (typically via additional loss terms) to learn meaningful solutions, e.g., cycle-consistency [9], entropic regularization [11] etc. In many cases, models need to be augmented with additional networks to enforce these biases during learning or for flexible inference at test time.

Latent variable generative models are highly effective for inferring hidden structure within observed data from a single domain [12]. For example, recent works have shown that these models can learn useful disentangled representations in a fully unsupervised manner [13, 14]. In this work, we present AlignFlow, a latent variable generative framework that seeks to discover the shared structure across

*Equal Contribution.
Preprint. Under review.

multiple data domains using normalizing flows [15–17]. AlignFlow models the data from each domain via an invertible generative model with a *single latent space shared across all the domains*. If we let the two domains to be A and B with a shared latent space, say Z, then the latent variable generative model for A may additionally share some or all parameters with the model of domain B. Akin to a single invertible model, the collection of invertible models in AlignFlow provide great flexibility in specifying learning objectives and can be trained via maximum likelihood estimation, adversarial training or a hybrid variant accounting for both objectives.

By virtue of an invertible design, AlignFlow naturally extends as a cross-domain translation model. To translate data across two domains, say A to B, we can invert a data point from $A \rightarrow Z$ first followed by a second inversion from $Z \rightarrow B$. Appealingly, we show that this composition of invertible mappings is *exactly cycle-consistent*, i.e., translating a datapoint from A to B using the forward mapping and backwards using the reverse mapping gives back the original datapoint and vice versa from B to A. Cycle-consistency was first introduced in CycleGAN [18] and has been shown to be an excellent inductive bias for underconstrained problems, such as unpaired domain alignment. While models such as CycleGAN only provide approximate cycle-consistency by incorporating additional loss terms, AlignFlow can omit these terms and guarantee exact cycle-consistency by design.

We analyze the AlignFlow framework extensively. Theoretically, we derive conditions under which the AlignFlow objective is consistent in the sense of recovering the true marginal distributions. Empirically, we consider two sets of tasks. In the first task, we demonstrate the ability of AlignFlow to effectively perform density estimation on a target domain given data from an additional related domain. Next, we compare AlignFlow against unsupervised domain adaptations based on cross-domain image translations and observe consistent improvements over 3 benchmark configurations.

2 Preliminaries

In this section, we discuss the necessary background and notation on generative adversarial networks and normalizing flows. We use uppercase notation X, Y, Z to denote random variables, and lowercase notation x, y, z to denote specific values in the italicized corresponding sample spaces $\mathcal{X}, \mathcal{Y}, \mathcal{Z}$.

2.1 Generative Adversarial Networks

A generative adversarial network (GAN) is a latent variable model which specifies a deterministic mapping $h : \mathcal{Z} \rightarrow \mathcal{X}$ between a set of latent variables Z and a set of observed variables X [19]. In order to sample from GANs, we need a prior density over Z that permits efficient sampling. A GAN generator can also be conditional, where the conditioning is on another set of observed variables (and optionally the latent variables Z as before) [20].

A GAN is trained via adversarial training, wherein the generator h plays a minimax game with an auxiliary critic C . The goal of the critic $C : \mathcal{X} \rightarrow \mathbb{R}$ is to distinguish real samples from the observed dataset with samples generated via h . The generator, on the other hand, tries to generate samples that can maximally confuse the critic. Many learning objectives have been proposed for adversarial training, including those based on f-divergences [21], Wasserstein Distance [22], and maximum mean discrepancy [23]. For the standard cross-entropy based GAN loss, the critic outputs a probability of a datapoint being real and optimizes the following objective w.r.t. a data distribution $p_X^* : \mathcal{X} \rightarrow \mathbb{R}_{\geq 0}$:

$$\mathcal{L}_{\text{GAN}}(C, h) := \mathbb{E}_{x \sim p_X^*} [\log C(x)] + \mathbb{E}_{z \sim p_Z} [\log(1 - C(h(z)))]. \quad (1)$$

for a suitable choice of prior density p_Z . The generator and the critic are both parameterized by deep neural networks and learned via alternating gradient-based optimization. Because adversarial training only requires samples from the generative model, it can be used to train generative models with intractable or ill-defined likelihoods [24]. In practice, such likelihood-free methods give excellent performance on sampling-based tasks unlike the alternative maximum likelihood estimation-based training criteria for learning generative models. However, these models are harder to train due to the alternating minimax optimization and suffer from issues such as mode collapse [25].

2.2 Normalizing Flows

Normalizing flows represent a latent variable generative model that specifies an *invertible* mapping $h : \mathcal{Z} \rightarrow \mathcal{X}$ between a set of latent variables Z and a set of observed variables X. Let p_X and p_Z denote

the marginal densities defined by the model over \mathcal{X} and \mathcal{Z} respectively. Using the change-of-variables formula, the marginal densities can be related as:

$$p_{\mathcal{X}}(x) = p_{\mathcal{Z}}(z) \left| \det \frac{\partial h^{-1}}{\partial \mathbf{X}} \right|_{\mathbf{X}=x} \quad (2)$$

where $z = h^{-1}(x)$ due to the invertibility constraints. Here, the second term on the RHS corresponds to the absolute value of the determinant of the Jacobian of the inverse transformation and signifies the change in volume when translating across the two sample spaces.

For evaluating likelihoods via the change-of-variables formula, we require efficient and tractable evaluation of the prior density, the inverse transformation h^{-1} , and the determinant of its Jacobian of h^{-1} . To draw a sample from this model, we perform ancestral sampling, i.e., we first sample a latent vector $z \sim p_{\mathcal{Z}}(z)$ and obtain the sampled vector as given by $x = h(z)$. This requires the ability to efficiently: (1) sample from the prior density and (2) evaluate the forward transformation h . Many transformations parameterized by deep neural networks that satisfy one or more of these criteria have been proposed in the recent literature on normalizing flows, e.g., NICE [16] and Autoregressive Flows [26, 27]. By suitable design of transformations, both likelihood evaluation and sampling can be performed efficiently, as in Real-NVP [17]. Consequently, a flow model can be trained efficiently via maximum likelihood estimation as well as likelihood-free adversarial training [28].

3 The AlignFlow Framework

In this section, we present the AlignFlow framework for learning generative models in the presence of unpaired data from multiple domains. For ease of presentation, we consider the case of two domains. Unless mentioned otherwise, our results naturally extend to more than two domains as well.

3.1 Problem Setup

The learning setting we consider is as follows. We are given unpaired datasets \mathcal{D}_A and \mathcal{D}_B from two domains A and B respectively, where the datapoints are assumed to be sampled i.i.d. from the true marginal p_A^* and p_B^* respectively. We are interested in learning models for two sets of distributions (a) the marginal likelihoods p_A and p_B for unconditional density estimation and sampling from domains A and B respectively, and (b) conditional distributions $p_{A|B}$ and $p_{B|A}$ for translating (i.e., conditional sampling) from $B \rightarrow A$ and $A \rightarrow B$ respectively.

Before presenting the AlignFlow framework, we note two observations. For task (a), simply having a dataset from the target domain is enough. However, given the easy availability of unpaired data, we hope to exploit the shared structure across related domains for sample-efficient learning. For task (b), we note that the problem is heavily underconstrained since we are only given data from the marginal distributions and hence, it is unclear how to learn the conditional distribution. However, the recent spate of empirical successes suggest certain inductive biases can learn useful conditional distributions for tasks such as cross-domain translation and domain adaptation even for this underconstrained problem [9, 29].

3.2 Representation

We will use a graphical model to represent the relationships between the domains. Consider a Bayesian network $A \leftarrow Z \rightarrow B$ with two sets of observed random variables A and B with domains $\mathcal{A} \subseteq \mathbb{R}^n$ and $\mathcal{B} \subseteq \mathbb{R}^n$ respectively, and a parent set of latent random variables Z with domain \mathcal{Z} .

The latent variables Z indicate a shared feature space between the observed variables A and B, which will be exploited later for efficient learning and inference. While Z is unobserved, we assume a prior density p_Z over these variables, such as an isotropic Gaussian. Finally, to compactly specify the joint distribution over all sets of variables, we constrain the relationship between A and Z, and B and Z to be invertible. That is, we specify mappings $G_{Z \rightarrow A}$ and $G_{Z \rightarrow B}$ such that the respective inverses $G_{A \rightarrow Z} = G_{Z \rightarrow A}^{-1}$ and $G_{B \rightarrow Z} = G_{Z \rightarrow B}^{-1}$ exist. Notice that such a representation naturally provides a mechanism to translate from one domain to another as the composition of two invertible mappings:

$$G_{A \rightarrow B} = G_{Z \rightarrow B} \circ G_{A \rightarrow Z} \quad (3)$$

$$G_{B \rightarrow A} = G_{Z \rightarrow A} \circ G_{B \rightarrow Z}. \quad (4)$$

Since composition of invertible mappings is invertible, both $G_{A \rightarrow B}$ and $G_{B \rightarrow A}$ are invertible. In fact, it is straightforward to observe that $G_{A \rightarrow B}$ and $G_{B \rightarrow A}$ are inverses of each other:

$$G_{A \rightarrow B}^{-1} = (G_{Z \rightarrow B} \circ G_{A \rightarrow Z})^{-1} = G_{A \rightarrow Z}^{-1} \circ G_{Z \rightarrow B}^{-1} = G_{Z \rightarrow A} \circ G_{B \rightarrow Z} = G_{B \rightarrow A}. \quad (5)$$

3.3 Learning Algorithms & Objectives

As discussed in the preliminaries, each of the individual flow models $Z \rightarrow A$ and $Z \rightarrow B$ express a model for p_A and p_B respectively and can be trained independently via maximum likelihood estimation, adversarial learning, or a hybrid objective. However, our goal is to perform sample-efficient learning by exploiting data from other domains as well as learn a conditional mapping across the two domains. For both these goals, we require learning algorithms which use data from both domains for parameter estimation. Unless mentioned otherwise, all our results that hold for a particular domain A will have a natural counterpart for the domain B.

Adversarial Training. Instead of generating data in domain A by sampling from the prior density p_Z , we can consider conditional sampling based on data sampled from domain B. That is, we introduce a critic C_A that plays a minimax game with the generator mapping $G_{B \rightarrow A}$ with the prior density given as p_B^* . The critic C_A distinguishes real samples $a \sim p_A^*$ with the generated samples $G_{B \rightarrow A}(b)$ for $b \sim p_B^*$. For example, the cross-entropy GAN loss in this case is given as:

$$\mathcal{L}_{\text{GAN}}(C_A, G_{B \rightarrow A}) = \mathbb{E}_{a \sim p_A^*}[\log C_A(a)] + \mathbb{E}_{b \sim p_B^*}[\log(1 - C_A(G_{B \rightarrow A}(b)))] \quad (6)$$

The expectation above are approximated empirically via datasets \mathcal{D}_A and \mathcal{D}_B respectively.

Maximum Likelihood Estimation. Unlike adversarial training, flow models trained with maximum likelihood estimation (MLE) explicitly require a prior p_Z with a tractable density to apply the change-of-variables formula. Due to the tractability requirement, we cannot substitute p_Z for p_B^* in this case. Instead, we propose to share parameters between the two mappings. The extent of parameter sharing depends on the similarity across the two domains; for highly similar domains, entire architectures could potentially be shared in which case $G_{Z \rightarrow A} = G_{Z \rightarrow B}$.

Hybrid Training. Both MLE and adversarial training objectives can be combined into a single training objective. In particular, the most expressive AlignFlow objective is given as:

$$\begin{aligned} \mathcal{L}_{\text{AlignFlow}}(G_{B \rightarrow A}, C_A, C_B; \lambda_A, \lambda_B) &= \mathcal{L}_{\text{GAN}}(C_A, G_{B \rightarrow A}) + \mathcal{L}_{\text{GAN}}(C_B, G_{A \rightarrow B}) \\ &\quad - \lambda_A \mathcal{L}_{\text{MLE}}(G_{Z \rightarrow A}) - \lambda_B \mathcal{L}_{\text{MLE}}(G_{Z \rightarrow B}) \end{aligned} \quad (7)$$

where $\lambda_A \geq 0$ and $\lambda_B \geq 0$ are hyperparameters that reflect the strength of the MLE terms for domains A and B respectively. The AlignFlow objective is minimized w.r.t. the parameters of the generator $G_{A \rightarrow B}$ and maximized w.r.t. parameters of the critics C_A and C_B . Notice that $\mathcal{L}_{\text{AlignFlow}}$ is a function of the critics C_A, C_B and only $G_{B \rightarrow A}$ since the latter also encompasses the other parametric functions appearing in the objective ($G_{A \rightarrow B}, G_{Z \rightarrow A}, G_{Z \rightarrow B}$) via the invertibility constraints in Eqs. 3-5. When $\lambda_A = \lambda_B = 0$, we perform pure *adversarial training* and the prior over Z plays no role in learning. On the other hand, when $\lambda_A = \lambda_B \rightarrow \infty$, we can perform pure *MLE training* to learn the invertible generator. Here, the critics C_A, C_B play no role since the adversarial training terms are ignored.

3.4 Inference

AlignFlow can be used for both conditional and unconditional sampling at test time. For conditional sampling as in the case of domain translation, we are given a datapoint $b \in \mathcal{B}$ and we can draw the corresponding cross-domain translation in domain \mathcal{A} via the mapping $G_{B \rightarrow A}$. For unconditional sampling, we require $\lambda_A \neq 0$ since doing so will activate the use of the prior p_Z via the MLE terms in the learning objective. Thereafter, we can obtain samples by first drawing $z \sim p_Z$ and then applying the mapping $G_{Z \rightarrow A}$ to z . Furthermore, the same z can be mapped to domain \mathcal{B} via $G_{Z \rightarrow B}$. Hence, we can sample paired data $(G_{Z \rightarrow A}(z), G_{Z \rightarrow B}(z))$ given $z \sim p_Z$.

4 Theoretical Analysis

The AlignFlow objective consists of three parametric models: one generator $G_{B \rightarrow A} \in \mathcal{G}$, and two critics $C_A \in \mathcal{C}_A, C_B \in \mathcal{C}_B$. Here, $\mathcal{G}, \mathcal{C}_A, \mathcal{C}_B$ denote model families specified e.g., via deep neural

network based architectures. In this section, we analyze the optimal solutions to these parameterized models within well-specified model families.

4.1 Optimal Generators

Our first result characterizes the conditions under which the optimal generators exhibit *marginal-consistency* for the data distributions defined over the domains A and B.

Definition 1. Let $p_{X,Y}$ denote the joint distribution between two domains \mathcal{X} and \mathcal{Y} . An invertible mapping $G_{Y \rightarrow X} : \mathcal{Y} \rightarrow \mathcal{X}$ is marginally-consistent w.r.t. two arbitrary distributions (p_X, p_Y) iff for all $x \in \mathcal{X}, y \in \mathcal{Y}$:

$$p_X(x) = \begin{cases} p_Y(y) \left| \det \frac{\partial G_{Y \rightarrow X}^{-1}}{\partial Y} \right|_{Y=y}, & \text{if } x = G_{Y \rightarrow X}(y) \\ 0, & \text{otherwise.} \end{cases} \quad (8)$$

Next, we show that AlignFlow is marginally-consistent for well-specified model families.

Lemma 1. Let \mathcal{G}_A and \mathcal{G}_B denote the class of invertible mappings represented by the AlignFlow architecture for mapping $Z \rightarrow A$ and $Z \rightarrow B$. For a given choice of prior distribution p_Z , if there exist mappings $G_{Z \rightarrow A}^* \in \mathcal{G}_A, G_{Z \rightarrow B}^* \in \mathcal{G}_B$ that are marginally consistent w.r.t. (p_A^*, p_Z) and (p_B^*, p_Z) respectively, then the mapping $G_{B \rightarrow A}^* = G_{Z \rightarrow A}^* \circ G_{Z \rightarrow B}^{*-1}$ is marginally-consistent w.r.t. (p_A^*, p_B^*) .

The result follows directly from Definition 1 and change-of-variables applied to the mapping $G_{B \rightarrow A}^*$.

Theorem 1. Assume that the model families for the critics $C_A : \mathcal{A} \rightarrow [0, 1]$ and $C_B : \mathcal{B} \rightarrow [0, 1]$ are the set of all measurable functions for the cross-entropy GAN objective. Then, $G_{B \rightarrow A}^*$ (as defined in Lemma 1) globally minimizes the AlignFlow objective in Eq. 7 for any value of $\lambda_A \geq 0, \lambda_B \geq 0$.

Proof. See Appendix A.1. Theorem 1 suggests that optimizing the AlignFlow objective will recover the marginal data distributions p_A^* and p_B^* under suitable conditions. For the other goal of learning cross-domain mappings, we note that marginally-consistent mappings w.r.t. a target data distribution (such as p_A^*) and a target prior density (such as p_B^*) need not be unique. While a cycle-consistent, invertible model family mitigates the underconstrained nature of the cross-domain translation problem, it does not provably eliminate it. We provide some non-identifiable constructions in Appendix A.3 and leave the exploration of additional constraints that guarantee identifiability to future work.

4.2 Optimal Critics

Unlike standard adversarial training of an unconditional normalizing flow model [28, 30], the AlignFlow model involves two critics. Here, we are interested in characterizing the dependence of the optimal critics for a given invertible mapping $G_{A \rightarrow B}$. Consider the AlignFlow framework where the GAN loss terms in Eq. 7 are specified via the cross-entropy objective in Eq. 6. For this model, we can relate the optimal critics using the following result.

Theorem 2. Let p_A^* and p_B^* denote the true data densities for domains \mathcal{A} and \mathcal{B} respectively. Let C_A^* and C_B^* denote the optimal critics for the AlignFlow objective with the cross-entropy GAN loss for any fixed choice of the invertible mapping $G_{A \rightarrow B}$. Letting $b = G_{A \rightarrow B}(a)$ for any $a \in \mathcal{A}$, we have:

$$C_A^*(a) = \frac{C_B^*(b)p_A^*(a)}{p_A^*(a) + p_B^*(b)(1 - C_B^*(b)) \left| \det \frac{\partial G_{A \rightarrow B}^{-1}}{\partial A} \right|_{A=a}}. \quad (9)$$

Proof. See Appendix A.2. In essence, the above result shows that the optimal critic for one domain, w.l.o.g. say A, can be directly obtained via the optimal critic of another domain B for any choice of the invertible mapping $G_{A \rightarrow B}$, assuming one were given access to the data marginals p_A^* and p_B^* .

4.3 Exact Cycle Consistency

So far, we have only discussed objectives that are marginal consistent with respect to data distributions p_A^* and p_B^* . However, many domain alignment tasks such as cross-domain translation require can be cast as learning a joint distribution $p_{A,B}^*$. As discussed previously, this problem is underconstrained given unpaired datasets \mathcal{D}_A and \mathcal{D}_B and the learned marginal densities alone do not guarantee learning

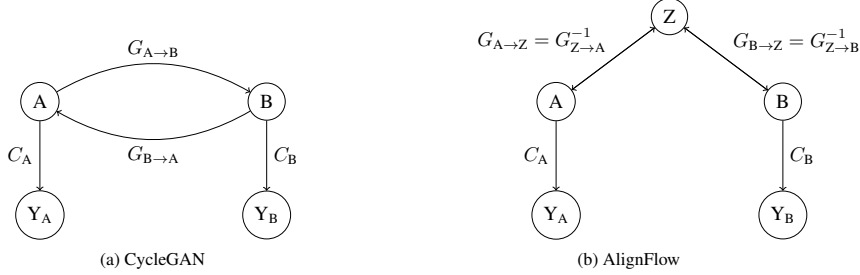


Figure 1: CycleGAN v.s. AlignFlow for unpaired cross-domain translation. Unlike CycleGAN, AlignFlow specifies a single invertible mapping $G_{A \rightarrow Z} \circ G_{B \rightarrow Z}^{-1}$ that is exactly cycle-consistent, represents a shared latent space Z between the two domains, and can be trained via both adversarial training and exact maximum likelihood estimation. Double-headed arrows denote invertible mappings. Y_A and Y_B are random variables denoting the output of the critics used for adversarial training.

a mapping that is useful for downstream tasks. Cycle consistency, as proposed in CycleGAN [18], is a highly effective learning objective that encourages learning of meaningful cross-domain mappings such that the data translated from domain \mathcal{A} to \mathcal{B} via $G_{A \rightarrow B}$ to be mapped back to the original datapoints in \mathcal{A} via $G_{B \rightarrow A}$. That is, $G_{B \rightarrow A}(G_{A \rightarrow B}(a)) \approx a$ for all $a \in \mathcal{A}$. Formally, the cycle-consistency loss for translation from A to B and back is defined as:

$$\mathcal{L}_{\text{Cycle}}(G_{B \rightarrow A}, G_{A \rightarrow B}) = E_{a \sim p_A^*} [\|G_{B \rightarrow A}(G_{A \rightarrow B}(a)) - a\|_1] \quad (10)$$

Symmetrically, a cycle consistency term $\mathcal{L}_{\text{Cycle}}(G_{A \rightarrow B}, G_{B \rightarrow A})$ in the reverse direction encourages $G_{A \rightarrow B}(G_{B \rightarrow A}(b)) \approx b$ for all $b \in \mathcal{B}$. Next, we show that AlignFlow is *exactly* cycle consistent.

Proposition 1. *Let \mathcal{G} denote the class of invertible mappings represented by an arbitrary AlignFlow architecture. For any $G_{B \rightarrow A} \in \mathcal{G}$, we have:*

$$\mathcal{L}_{\text{Cycle}}(G_{B \rightarrow A}, G_{A \rightarrow B}) = 0 \quad (11)$$

$$\mathcal{L}_{\text{Cycle}}(G_{A \rightarrow B}, G_{B \rightarrow A}) = 0 \quad (12)$$

where $G_{A \rightarrow B} = G_{B \rightarrow A}^{-1}$ by design.

The proposition follows directly from the invertible design of the AlignFlow framework (Eq. 5).

Comparison with CycleGAN. We illustrate and compare AlignFlow and CycleGAN in Figure 1. CycleGAN parameterizes two independent cross-domain mappings $G_{A \rightarrow B}$ and $G_{B \rightarrow A}$, whereas AlignFlow only specifies a single, invertible mapping. Learning in a CycleGAN is restricted to an adversarial training objective along with cycle-consistent loss terms, whereas AlignFlow is exactly consistent and can be trained via adversarial learning, MLE, or a hybrid (Eq. 7) without the need for additional loss terms to enforce cycle consistency. Finally, inference in CycleGAN is restricted to conditional sampling since it does not involve any latent variables Z with easy-to-sample prior densities. As described previously, AlignFlow permits both conditional and unconditional sampling.

Comparison with UNIT and CoGAN. Models such as CoGAN [31] and its extension UNIT [29] also consider adding a shared-space constraint between two decoders decoding into the different domains. These models again can only enforce approximate cycle consistency, introduce additional encoders, and approximate lower bounds to the log-likelihood thereby prohibiting exact MLE training.

5 Experimental Evaluation

To achieve our two goals of data-efficient modeling of individual domains and effective cross-domain mappings, we evaluate AlignFlow on two tasks: (a) density estimation given data from multiple domains, and (b) unsupervised domain adaptation. For additional experimental details and analysis beyond those stated below, we refer the reader to Appendix B.

5.1 Data-efficient Density Estimation via pure MLE Training

In multi-domain density estimation, we are given data from two domains. The target domain is a data-limited domain which we augment with additional data from a related, but different domain.



Figure 2: Generated samples and held-out negative log-likelihoods (NLL, in bits/dimension or bpd) for MLE training on the CIFAR-10 dataset alone (left) and augmented with CIFAR-100 (right).

Table 1: Test classification accuracies for domain adaptation from source→target. The source only and target only models directly use classifiers trained on the source and target datasets respectively. Baseline numbers directly reported from the cited works.

Model	MNIST→USPS	USPS→MNIST	SVHN→MNIST
source only	82.2 ± 0.8	69.6 ± 3.8	67.1 ± 0.6
ADDA [34]	89.4 ± 0.2	90.1 ± 0.8	76.0 ± 1.8
CyCADA [3]	95.6 ± 0.2	96.5 ± 0.1	90.4 ± 0.4
UNIT [29]	95.97	93.58	90.53
AlignFlow	96.2 ± 0.2	96.7 ± 0.1	91.0 ± 0.3
target only	96.3 ± 0.1	99.2 ± 0.1	99.2 ± 0.1

The goal is to learn a single generative model for the target domain using one or both datasets. We ignore the adversarial learning terms for AlignFlow in this experiment since the density estimation objective is directly related to MLE.

We experimented with the CIFAR-10 dataset using a simplified Glow architecture [32]. For the augmented dataset during training, we consider CIFAR-100 and ImageNet downsampled to 32x32 [33]. CIFAR-100 is obtained from the same source dataset of the 80 million tiny images dataset but has non-overlapping classes with those of CIFAR-10 and hence, can be viewed as a different data distribution. ImageNet is derived from a different source than CIFAR-10. In Figure 2, we show the samples and held-out negative log-likelihoods of the best performing models. We defer samples with ImageNet augmentation to Appendix B.1, where we achieve NLL of 3.45 bpd. A baseline approach which ignores the data available from the augmented domains underperforms and training AlignFlow using pure MLE with weight sharing can effectively exploit data from related domains.

5.2 Unsupervised Domain Adaptation via pure Adversarial Training

In unsupervised domain adaptation [10], we are given data from two related domains: a source and a target domain. For the source, we have access to both the input datapoints and their labels. For the target, we are only provided with input datapoints without any labels. Using the available data, the goal is to learn a classifier for the target domain. We extend [3] to use an AlignFlow architecture and objective (adversarially trained Real-NVPs [17] here) in place of CycleGAN for this task.

A variety of algorithms have been proposed for the above task which seek to match pixel-level or feature-level distributions across the two domains. See Appendix B.3 for more details. For fair comparison, we compare against baselines Cycada [3] and UNIT [29] which involve pixel-level translations and are closest to the current work. We evaluate across all pairs of source and target datasets as in [3] and [29]: MNIST [35], USPS [36], SVHN [37], which are all image datasets of handwritten digits with 10 classes. In Table 1, we see that AlignFlow outperforms both Cycada [3]

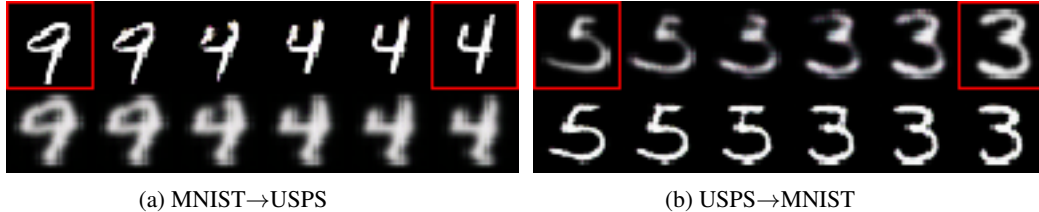


Figure 3: Multi-domain latent space interpolations. **Top:** Left-most and right-most images are sampled from \mathcal{D}_A (in red boxes). Interpolation is then performed in latent space and then decoded using $G_{Z \rightarrow A}$. **Bottom:** For each corresponding image in the top row, its latent representation is decoded into the target domain using $G_{Z \rightarrow B}$. Note how both class identity and style are preserved in the interpolated pairs of digits in the two domains. Also, notice that the USPS images (even the true ones in red boxes) are slightly blurred due to the upscaling applied as standard preprocessing.

(based on CycleGAN) and UNIT [29] in all cases. This also suggests that combining AlignFlow with recent state-of-the-art adaptation approaches e.g., [38–43] is an interesting direction for future work.

5.3 Multi-domain Latent Interpolations via Hybrid Training

The use of a shared latent space in AlignFlow allows us to perform paired interpolations in two domains simultaneously. While pure MLE without any parameter sharing does not give good alignment, pure adversarial training cannot be used for unconditional sampling since the prior p_Z is inactive. Hence, we use AlignFlow models trained via a hybrid objective for latent space interpolations. In particular, we sample two datapoints $a', a'' \in \mathcal{D}_A$ and obtain their latent representations $z', z'' \in \mathcal{Z}$ via $G_{Z \rightarrow A}$. Following [17], we compute interpolations in the polar space as $\tilde{z} = z' \sin \phi + z'' \cos \phi$ for several values of $\phi \in (0, 2\pi)$. Finally, we map \tilde{z} to either back to domain A via $G_{Z \rightarrow A}$ and B via $G_{Z \rightarrow B}$. We show this empirically on the MNIST/USPS datasets in Figure 3. We see that many aspects of style and content are preserved in the samples corresponding to the latent space interpolations.

6 Related Work

A key assumption in unsupervised domain alignment is the existence of a deterministic or stochastic mapping $G_{A \rightarrow B}$ such that the distribution of B matches that of $G_{A \rightarrow B}(A)$, and vice versa. This assumption can be incorporated as a marginal distribution-matching constraint into the objective using an adversarially-trained GAN critic [19]. However, this objective is under-constrained. To partially mitigate this issue, CycleGAN [18], DiscoGAN [1], and DualGAN [44] added an approximate cycle-consistency constraint that encourages $G_{B \rightarrow A} \circ G_{A \rightarrow B}$ and $G_{A \rightarrow B} \circ G_{B \rightarrow A}$ to behave like identity functions on domains A and B respectively. While cycle-consistency is empirically very effective, alternatives based on variational autoencoders that do not require either cycles or adversarial training have also been proposed recently [45, 46].

Models such as CoGAN [31], UNIT [29], and CycleGAN [18] have since been extended to enable one-to-many mappings [9, 47] as well as multi-domain alignment [48]. Our work focuses on the one-to-one unsupervised domain alignment setting. In contrast to previous models, AlignFlow leverages both a shared latent space and *exact* cycle-consistency. To our knowledge, AlignFlow provides the first demonstration that invertible models can be used successfully in lieu of the cycle-consistency objective. Furthermore, AlignFlow allows the incorporation of exact maximum likelihood training, which we demonstrated to induce a meaningful shared latent space that is amenable to interpolation.

7 Conclusion & Future Work

We presented AlignFlow, a generative framework for learning from multiple data sources based on normalizing flow models. The use of normalizing flow models is an attractive choice for several reasons we highlight: it guarantees exact cycle-consistency via a single cross-domain mapping, learns a shared latent space across two domains, and permits a flexible training objective which is a hybrid of terms corresponding to adversarial training and exact maximum likelihood estimation. Theoretically, we derived conditions under which the AlignFlow model learns marginals that are consistent with the underlying data distributions. Finally, our empirical evaluation demonstrated significant gains on the

tasks of multi-domain density estimation and unsupervised domain adaptation, and an increase in inference capabilities, e.g., paired interpolations in the latent space for two domains.

In the future, we plan to consider extensions of AlignFlow for learning stochastic, multimodal mappings [9] and translations across more than two domains [48]. Exploring recent advancements in invertible architectures [13, 26, 27, 49–52] for improved learning of AlignFlow is another promising direction. In spite of strong empirical results in domain alignment, theories explaining such results are limited [53–57]. With a handle on model likelihoods and invertible inference, we are optimistic that AlignFlow can potentially aid the development of such a theory and characterize useful structure for guaranteeing identifiability in underconstrained problems involving multiple domains.

References

- [1] Taeksoo Kim, Moon-su Cha, Hyunsoo Kim, Jung Kwon Lee, and Jiwon Kim. Learning to discover cross-domain relations with generative adversarial networks. *arXiv preprint arXiv:1703.05192*, 2017.
- [2] Yaniv Taigman, Adam Polyak, and Lior Wolf. Unsupervised cross-domain image generation. *arXiv preprint arXiv:1611.02200*, 2016.
- [3] Judy Hoffman, Eric Tzeng, Taesung Park, Jun-Yan Zhu, Phillip Isola, Kate Saenko, Alexei A Efros, and Trevor Darrell. Cycada: Cycle-consistent adversarial domain adaptation. *arXiv preprint arXiv:1711.03213*, 2017.
- [4] Konstantinos Bousmalis, Nathan Silberman, David Dohan, Dumitru Erhan, and Dilip Krishnan. Unsupervised pixel-level domain adaptation with generative adversarial networks. In *IEEE Conference on Computer Vision and Pattern Recognition*, 2017.
- [5] Phillip Isola, Jun-Yan Zhu, Tinghui Zhou, and Alexei A Efros. Image-to-image translation with conditional adversarial networks. In *IEEE Conference on Computer Vision and Pattern Recognition*. IEEE, 2017.
- [6] Ting-Chun Wang, Ming-Yu Liu, Jun-Yan Zhu, Guilin Liu, Andrew Tao, Jan Kautz, and Bryan Catanzaro. Video-to-video synthesis. *arXiv preprint arXiv:1808.06601*, 2018.
- [7] Guillaume Lample, Alexis Conneau, Ludovic Denoyer, and Marc’Aurelio Ranzato. Unsupervised machine translation using monolingual corpora only. *arXiv preprint arXiv:1711.00043*, 2017.
- [8] Jiatao Gu, Hany Hassan, Jacob Devlin, and Victor OK Li. Universal neural machine translation for extremely low resource languages. *arXiv preprint arXiv:1802.05368*, 2018.
- [9] Jun-Yan Zhu, Richard Zhang, Deepak Pathak, Trevor Darrell, Alexei A Efros, Oliver Wang, and Eli Shechtman. Toward multimodal image-to-image translation. In *Advances in Neural Information Processing Systems*, 2017.
- [10] Kate Saenko, Brian Kulis, Mario Fritz, and Trevor Darrell. Adapting visual category models to new domains. In *European conference on computer vision*. Springer, 2010.
- [11] Nicolas Courty, Rémi Flamary, Amaury Habrard, and Alain Rakotomamonjy. Joint distribution optimal transportation for domain adaptation. In *Advances in Neural Information Processing Systems*, pages 3730–3739, 2017.
- [12] David M Blei, Andrew Y Ng, and Michael I Jordan. Latent dirichlet allocation. *Journal of machine Learning research*, 3(Jan):993–1022, 2003.
- [13] Tian Qi Chen, Yulia Rubanova, Jesse Bettencourt, and David K Duvenaud. Neural ordinary differential equations. In *Advances in Neural Information Processing Systems*, 2018.
- [14] Irina Higgins, Loic Matthey, Arka Pal, Christopher Burgess, Xavier Glorot, Matthew Botvinick, Shakir Mohamed, and Alexander Lerchner. beta-vae: Learning basic visual concepts with a constrained variational framework. In *International Conference on Learning Representations*, volume 3, 2017.

- [15] Danilo Jimenez Rezende and Shakir Mohamed. Variational inference with normalizing flows. *arXiv preprint arXiv:1505.05770*, 2015.
- [16] Laurent Dinh, David Krueger, and Yoshua Bengio. Nice: Non-linear independent components estimation. *arXiv preprint arXiv:1410.8516*, 2014.
- [17] Laurent Dinh, Jascha Sohl-Dickstein, and Samy Bengio. Density estimation using real nvp. *arXiv preprint arXiv:1605.08803*, 2017.
- [18] Jun-Yan Zhu, Taesung Park, Phillip Isola, and Alexei A Efros. Unpaired image-to-image translation using cycle-consistent adversarial networks. In *International Conference on Computer Vision*, 2017.
- [19] Ian Goodfellow, Jean Pouget-Abadie, Mehdi Mirza, Bing Xu, David Warde-Farley, Sherjil Ozair, Aaron Courville, and Yoshua Bengio. Generative adversarial nets. In *Advances in neural information processing systems*, 2014.
- [20] Mehdi Mirza and Simon Osindero. Conditional generative adversarial nets. *arXiv preprint arXiv:1411.1784*, 2014.
- [21] Sebastian Nowozin, Botond Cseke, and Ryota Tomioka. f-gan: Training generative neural samplers using variational divergence minimization. In *Advances in Neural Information Processing Systems*, 2016.
- [22] Martin Arjovsky, Soumith Chintala, and Léon Bottou. Wasserstein gan. In *International Conference on Machine Learning*, 2017.
- [23] Chun-Liang Li, Wei-Cheng Chang, Yu Cheng, Yiming Yang, and Barnabás Póczos. Mmd gan: Towards deeper understanding of moment matching network. In *Advances in Neural Information Processing Systems*, 2017.
- [24] Shakir Mohamed and Balaji Lakshminarayanan. Learning in implicit generative models. *arXiv preprint arXiv:1610.03483*, 2016.
- [25] Ian Goodfellow. Nips 2016 tutorial: Generative adversarial networks. *arXiv preprint arXiv:1701.00160*, 2016.
- [26] Diederik P Kingma, Tim Salimans, Rafal Jozefowicz, Xi Chen, Ilya Sutskever, and Max Welling. Improved variational inference with inverse autoregressive flow. In *Advances in Neural Information Processing Systems*, 2016.
- [27] George Papamakarios, Iain Murray, and Theo Pavlakou. Masked autoregressive flow for density estimation. In *Advances in Neural Information Processing Systems*, 2017.
- [28] Aditya Grover, Manik Dhar, and Stefano Ermon. Flow-gan: Combining maximum likelihood and adversarial learning in generative models. In *AAAI Conference on Artificial Intelligence*, 2018.
- [29] Ming-Yu Liu, Thomas Breuel, and Jan Kautz. Unsupervised image-to-image translation networks. In *Advances in Neural Information Processing Systems*, 2017.
- [30] Ivo Danihelka, Balaji Lakshminarayanan, Benigno Uribe, Daan Wierstra, and Peter Dayan. Comparison of maximum likelihood and gan-based training of real nvps. *arXiv preprint arXiv:1705.05263*, 2017.
- [31] Ming-Yu Liu and Onsel Tuzel. Coupled generative adversarial networks. In *Advances in neural information processing systems*, 2016.
- [32] Diederik P Kingma and Prafulla Dhariwal. Glow: Generative flow with invertible 1x1 convolutions. *arXiv preprint arXiv:1807.03039*, 2018.
- [33] Aaron van den Oord, Nal Kalchbrenner, and Koray Kavukcuoglu. Pixel recurrent neural networks. *arXiv preprint arXiv:1601.06759*, 2016.

- [34] Eric Tzeng, Judy Hoffman, Kate Saenko, and Trevor Darrell. Adversarial discriminative domain adaptation. In *IEEE Conference on Computer Vision and Pattern Recognition*, 2017.
- [35] Yann LeCun, Léon Bottou, Yoshua Bengio, Patrick Haffner, et al. Gradient-based learning applied to document recognition. *Proceedings of the IEEE*, 86(11):2278–2324, 1998.
- [36] Jonathan J. Hull. A database for handwritten text recognition research. *IEEE Transactions on pattern analysis and machine intelligence*, 16(5):550–554, 1994.
- [37] Yuval Netzer, Tao Wang, Adam Coates, Alessandro Bissacco, Bo Wu, and Andrew Y Ng. Reading digits in natural images with unsupervised feature learning. *NIPS Workshop on Deep Learning and Unsupervised Feature Learning*, 2011.
- [38] Rui Shu, Hung H Bui, Hirokazu Narui, and Stefano Ermon. A dirt-t approach to unsupervised domain adaptation. *arXiv preprint arXiv:1802.08735*, 2018.
- [39] Mingsheng Long, Zhangjie Cao, Jianmin Wang, and Michael I Jordan. Conditional adversarial domain adaptation. In *Advances in Neural Information Processing Systems*, pages 1640–1650, 2018.
- [40] Abhishek Kumar, Prasanna Sattigeri, Kahini Wadhawan, Leonid Karlinsky, Rogerio Feris, Bill Freeman, and Gregory Wornell. Co-regularized alignment for unsupervised domain adaptation. In *Advances in Neural Information Processing Systems*, pages 9345–9356, 2018.
- [41] Alexander H Liu, Yen-Cheng Liu, Yu-Ying Yeh, and Yu-Chiang Frank Wang. A unified feature disentangler for multi-domain image translation and manipulation. In *Advances in Neural Information Processing Systems*, pages 2590–2599, 2018.
- [42] Swami Sankaranarayanan, Yogesh Balaji, Carlos D Castillo, and Rama Chellappa. Generate to adapt: Aligning domains using generative adversarial networks. In *IEEE Conference on Computer Vision and Pattern Recognition*, 2018.
- [43] Yen-Cheng Liu, Yu-Ying Yeh, Tzu-Chien Fu, Sheng-De Wang, Wei-Chen Chiu, and Yu-Chiang Frank Wang. Detach and adapt: Learning cross-domain disentangled deep representation. In *IEEE Conference on Computer Vision and Pattern Recognition*, 2018.
- [44] Zili Yi, Hao Zhang, Ping Tan, and Minglun Gong. Dualgan: Unsupervised dual learning for image-to-image translation. In *International Conference on Computer Vision*, 2017.
- [45] Yedid Hoshen. Non-adversarial mapping with vaes. In *Advances in Neural Information Processing Systems*, 2018.
- [46] Yedid Hoshen and Lior Wolf. Nam: Non-adversarial unsupervised domain mapping. In *European Conference on Computer Vision*, 2018.
- [47] Xun Huang, Ming-Yu Liu, Serge Belongie, and Jan Kautz. Multimodal unsupervised image-to-image translation. *arXiv preprint arXiv:1804.04732*, 2018.
- [48] Yunje Choi, Minje Choi, Munyoung Kim, Jung-Woo Ha, Sunghun Kim, and Jaegul Choo. Stargan: Unified generative adversarial networks for multi-domain image-to-image translation. In *IEEE Conference on Computer Vision and Pattern Recognition*, 2018.
- [49] Jonathan Ho, Xi Chen, Aravind Srinivas, Yan Duan, and Pieter Abbeel. Flow++: Improving flow-based generative models with variational dequantization and architecture design. *arXiv preprint arXiv:1902.00275*, 2019.
- [50] Chin-Wei Huang, David Krueger, Alexandre Lacoste, and Aaron Courville. Neural autoregressive flows. *arXiv preprint arXiv:1804.00779*, 2018.
- [51] Will Grathwohl, Ricky TQ Chen, Jesse Bettencourt, Ilya Sutskever, and David Duvenaud. Ffjord: Free-form continuous dynamics for scalable reversible generative models. *arXiv preprint arXiv:1810.01367*, 2018.
- [52] Rianne van den Berg, Leonard Hasenclever, Jakub M Tomczak, and Max Welling. Sylvester normalizing flows for variational inference. *arXiv preprint arXiv:1803.05649*, 2018.

- [53] Tomer Galanti, Lior Wolf, and Sagie Benaim. The role of minimal complexity functions in unsupervised learning of semantic mappings. *arXiv preprint arXiv:1709.00074*, 2017.
- [54] Tomer Galanti, Sagie Benaim, and Lior Wolf. Generalization bounds for unsupervised cross-domain mapping with wgans. *arXiv preprint arXiv:1807.08501*, 2018.
- [55] David Alvarez-Melis, Stefanie Jegelka, and Tommi S Jaakkola. Towards optimal transport with global invariances. *arXiv preprint arXiv:1806.09277*, 2018.
- [56] Yifan Wu, Ezra Winston, Divyansh Kaushik, and Zachary Lipton. Domain adaptation with asymmetrically-relaxed distribution alignment. *arXiv preprint arXiv:1903.01689*, 2019.
- [57] Zhen Cui, Hong Chang, Shiguang Shan, and Xilin Chen. Generalized unsupervised manifold alignment. In *Advances in Neural Information Processing Systems*, 2014.
- [58] Adam Paszke, Sam Gross, Soumith Chintala, Gregory Chanan, Edward Yang, Zachary DeVito, Zeming Lin, Alban Desmaison, Luca Antiga, and Adam Lerer. Automatic differentiation in pytorch. 2017.
- [59] Marius Cordts, Mohamed Omran, Sebastian Ramos, Timo Rehfeld, Markus Enzweiler, Rodrigo Benenson, Uwe Franke, Stefan Roth, and Bernt Schiele. The cityscapes dataset for semantic urban scene understanding. In *IEEE Conference on Computer Vision and Pattern Recognition*, 2016.
- [60] Diederik P Kingma and Jimmy Ba. Adam: A method for stochastic optimization. *arXiv preprint arXiv:1412.6980*, 2014.
- [61] Tim Salimans and Durk P Kingma. Weight normalization: A simple reparameterization to accelerate training of deep neural networks. In *Advances in Neural Information Processing Systems*, 2016.
- [62] Kaiming He, Xiangyu Zhang, Shaoqing Ren, and Jian Sun. Deep residual learning for image recognition. In *IEEE Conference on Computer Vision and Pattern Recognition*, 2016.
- [63] Yaroslav Ganin and Victor Lempitsky. Unsupervised domain adaptation by backpropagation. *arXiv preprint arXiv:1409.7495*, 2014.

Appendices

A Proofs of Theoretical Results

A.1 Proof of Theorem 1

Proof. Since the maximum likelihood estimate minimizes the KL divergence between the data and model distributions, the optimal value for $\mathcal{L}_{\text{MLE}}(G_{Z \rightarrow A})$ is attained at a marginally-consistent mapping, say $G_{Z \rightarrow A}^*$. Symmetrically, there exists a marginally-consistent mapping $G_{Z \rightarrow B}^*$ that optimizes $\mathcal{L}_{\text{MLE}}(G_{Z \rightarrow B})$.

From Theorem 1 of Goodfellow et al. [19], we know that the cross-entropy GAN objective $\mathcal{L}_{\text{GAN}}(C_A, G_{B \rightarrow A})$ is globally minimized when $p_A = p_A^*$ and critic is Bayes optimal. Further, from Lemma 1, we know that $G_{B \rightarrow A}^*$ is marginally-consistent w.r.t. (p_A^*, p_B^*) . Hence, $G_{B \rightarrow A}^*$ globally minimizes $\mathcal{L}_{\text{GAN}}(C_A, G_{B \rightarrow A})$. Symmetrically, $G_{A \rightarrow B}^* = G_{B \rightarrow A}^{*-1}$ globally minimizes $\mathcal{L}_{\text{GAN}}(C_B, G_{A \rightarrow B})$.

Since $G_{B \rightarrow A}^* = G_{Z \rightarrow A}^* \circ G_{Z \rightarrow B}^{*-1}$ globally optimizes all the individual loss terms in the AlignFlow objective in Eq. 7, it globally optimizes the overall objective for any value of $\lambda_A \geq 0, \lambda_B \geq 0$. \square

A.2 Proof of Theorem 2

Proof. First, we note that only the GAN loss terms depend on C_A and C_B . Hence, the MLE terms are constants for a fixed $G_{B \rightarrow A}$ and hence, can be ignored for deriving the optimal critics. Next, for any GAN trained with the cross-entropy loss as specified in Eq 6, we know that the Bayes optimal critic C_A^* prediction for any $a \in \mathcal{A}$ is given as:

$$C_A^*(a) = \frac{p_A^*(a)}{p_A^*(a) + p_A(a)} \quad (13)$$

See Proposition 1 in Goodfellow et al. [19] for a proof.

We can relate the densities $p_A(a)$ and $p_B(b)$ via the change of variables as:

$$p_A(a) = p_B(b) \left| \det \frac{\partial G_{A \rightarrow B}^{-1}}{\partial A} \right|_{A=a} \quad (14)$$

where $b = G_{A \rightarrow B}(a)$.

Substituting the expression for density of $p_A(a)$ from Eq. 14 in Eq. 13, we get:

$$C_A^*(a) = \frac{p_A^*(a)}{p_A^*(a) + p_B(b) \left| \det \frac{\partial G_{A \rightarrow B}^{-1}}{\partial A} \right|_{A=a}} \quad (15)$$

where $b = G_{A \rightarrow B}(a)$.

Symmetrically, using Proposition 1 in Goodfellow et al. [19] we have the Bayes optimal critic C_B^* for any $b \in \mathcal{B}$ given as:

$$C_B^*(b) = \frac{p_B^*(b)}{p_B^*(b) + p_B(b)}. \quad (16)$$

Rearranging terms in Eq. 16, we have:

$$p_B(b) = p_B^*(b) \left(\frac{1}{C_B^*(b)} - 1 \right) \quad (17)$$

for any $b \in \mathcal{B}$.

Substituting the expression for density of $p_B(b)$ from Eq. 17 in Eq. 15, we get:

$$C_A^*(a) = \frac{C_B^*(b) p_A^*(a)}{p_A^*(a) + p_B^*(b) (1 - C_B^*(b)) \left| \det \frac{\partial G_{A \rightarrow B}^{-1}}{\partial A} \right|_{A=a}} \quad (18)$$

where $b = G_{A \rightarrow B}(a)$. \square

A.3 Non-identifiability of Cross-domain Mappings

As discussed, marginal consistency along with invertibility can only reduce the underconstrained nature of the unpaired cross-domain translation problem, but not completely eliminate it. In the following result, we identify one such class of non-identifiable model families for the MLE-only objective of AlignFlow ($\lambda_A = \infty, \lambda_B = \infty$). We will need the following definitions.

Definition 2. Let \mathcal{S}_n denotes the symmetric group on n dimensional permutation matrices. A function class for the cross-domain mappings \mathcal{G} is closed under permutations iff for all $G_{B \rightarrow A} \in \mathcal{G}, S \in \mathcal{S}_n$, we have $G_{B \rightarrow A} \circ S \in \mathcal{G}$.

Definition 3. A density p_X is symmetric iff for all $x \in \mathcal{X} \subseteq \mathbb{R}^n, S \in \mathcal{S}_n$, we have $p_X(x) = p_X(Sx)$.

Examples of distributions with symmetric densities include the isotropic Gaussian and Laplacian distributions.

Proposition 2. Consider the case where $G_{B \rightarrow A}^* \in \mathcal{G}$, and \mathcal{G} is closed under permutations. For a symmetric prior p_Z (e.g., isotropic Gaussian), there exists an optimal solution $G_{B \rightarrow A}^\dagger \in \mathcal{G}$ to the AlignFlow objective (Eq. 7) for $\lambda_A = \lambda_B = \infty$ such that $G_{B \rightarrow A}^\dagger \neq G_{B \rightarrow A}^*$.

Proof. We will prove the proposition via contradiction. That is, let's assume that $G_{B \rightarrow A}^*$ is a unique solution for the AlignFlow objective for $\lambda_A = \lambda_B = \infty$ (Eq. 7). Now, consider an alternate mapping $G_{B \rightarrow A}^\dagger = G_{B \rightarrow A}^* S$ for an arbitrary non-identity permutation matrix $S \neq I$ in the symmetric group.

As before, we note that $G_{B \rightarrow A}^* = G_{Z \rightarrow A}^* \circ G_{Z \rightarrow B}^{*-1}$ and $G_{B \rightarrow A}^\dagger = G_{Z \rightarrow A}^\dagger \circ G_{Z \rightarrow B}^{\dagger-1}$ due to the invertibility constraints in Eqs. 3-5. Since permutation matrices are invertible and so is $G_{B \rightarrow A}^*$, their composition given by $G_{B \rightarrow A}^\dagger$ is also invertible. Further, since \mathcal{G} is closed under permutation and $G_{B \rightarrow A}^* \in \mathcal{G}$, we also have $G_{B \rightarrow A}^\dagger \in \mathcal{G}$.

Next, we note that the inverse of a permutation matrix is also a permutation matrix. Since the prior is assumed to be symmetric and a transformation specified by a permutation matrix is volume-preserving (i.e., $\det(S) = 1$ for all $S \in \mathcal{S}_n$), we can use the change-of-variables formula in Eq. 2 to get:

$$\mathcal{L}_{\text{MLE}}(G_{Z \rightarrow A}^*) = \mathcal{L}_{\text{MLE}}(G_{Z \rightarrow A}^\dagger) \quad (19)$$

$$\mathcal{L}_{\text{MLE}}(G_{Z \rightarrow B}^*) = \mathcal{L}_{\text{MLE}}(G_{Z \rightarrow B}^\dagger). \quad (20)$$

Noting that $G_{B \rightarrow A}^* = G_{Z \rightarrow A}^* \circ G_{Z \rightarrow B}^{*-1}$ and $G_{B \rightarrow A}^\dagger = G_{Z \rightarrow A}^\dagger \circ G_{Z \rightarrow B}^{\dagger-1}$ due to the invertibility constraints in Eqs. 3-5, we can substitute the above equations in Eq. 7. When $\lambda_A = \lambda_B = \infty$, for any choice of C_A, C_B we have:

$$\begin{aligned} & \mathcal{L}_{\text{AlignFlow}}(G_{B \rightarrow A}^*, C_A, C_B, \lambda_A = \infty, \lambda_B = \infty) \\ &= \mathcal{L}_{\text{AlignFlow}}(G_{B \rightarrow A}^\dagger, C_A, C_B, \lambda_A = \infty, \lambda_B = \infty). \end{aligned} \quad (21)$$

The above equation implies that $G_{B \rightarrow A}^\dagger$ is also an optimal solution to the AlignFlow objective in Eq. 7 for $\lambda_A = \lambda_B = \infty$. Thus, we arrive at a contradiction since $G_{B \rightarrow A}^*$ is not the unique maximizer. Hence, proved. \square

The above construction suggests that MLE-only training can fail to identify the optimal mapping corresponding to the joint distribution $p_{A,B}^*$ even if it lies within the mappings represented via the family represented via the AlignFlow architecture. Failure modes due to non-identifiability could also potentially arise for adversarial and hybrid training. Empirically, we find that while MLE-only training gives poor performance for cross-domain translations, the hybrid and adversarial training objectives are much more effective, which suggests that these objectives are less susceptible to identifiability issues in recovering the true mapping.

B Experiment Details

We used PyTorch [58] for implementing our codebase. All models were trained on a single Nvidia TitanX GPU. We are attaching our anonymized code with the supplementary material and will make it publicly available at the end of the review process.

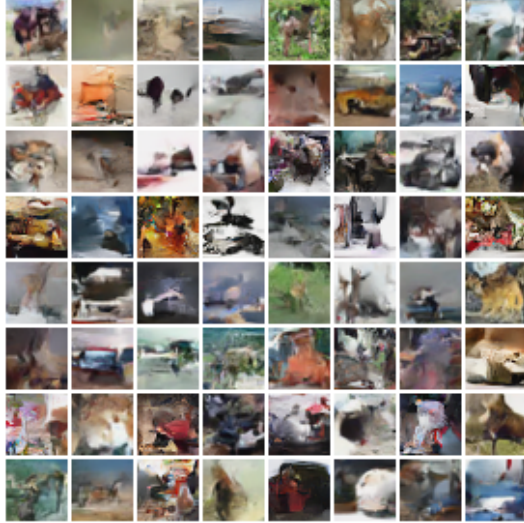


Figure 4: With ImageNet: 3.45 bpd

B.1 Density Estimation

Figure 4 shows the samples obtained by augmenting the CIFAR-10 dataset with ImageNet data. For these experiments, we shared all sets of parameters across the generators for the two domains (to keep number of parameters fixed across all approaches) and performed a hyperparameter search for the weight of the MLE objective for the augmented dataset. We searched over relative weights in $\{0.05, 0.1, 0.2, 0.5, 0.9, 1.0\}$.

The Glow architecture used in these experiments is the one used by Kingma and Dhariwal [32] for CIFAR-10 experiments which, in the notation of [32], corresponds to $K = 32$, $L = 3$, and $C = 512$. We now give a brief explanation of these hyperparameters: The Glow architecture consists of *levels*, which are sequences of transformations that process their inputs at the same spatial scale. The number of levels is denoted by L , and following [32] we use $L = 3$ for all CIFAR-10 experiments. Each level consists of K *flow steps* (we use $K = 32$), and each flow step has three parts: (1) activation normalization, (2) invertible 1×1 convolution, and (3) affine coupling in which half of the channels are used to compute an affine transformation applied to the remaining channels. In the affine coupling layers, one must choose the function for computing the scale and translate factors: Following [32], we use a simple 3-layer CNN with 512 channels ($C = 512$). We note that in contrast with prior works such as Real NVP [17], the Glow architecture does not make use of checkerboard masks in the coupling layers, instead using only channelwise masks.

Due to computational constraints, we run the full-scale Glow model on a single NVIDIA TitanX GPU for a batch size of 32, as opposed to the original multi-GPU model of [32] run with a batch size of 512. In any case, the goal of this experiment differs in the sense of demonstrating relative improvements via augmented data from a related domain, when methods are compared under a fixed computational budget and model size. The remaining training procedures are standard and match that of [32].

B.2 Image-To-Image Translation

In additional preliminary results on image-to-image translation tasks, we evaluate AlignFlow on three image-to-image translation datasets used by Zhu et al. [18]: Facades, Maps, and CityScapes [59]. These datasets are chosen because they provide one-to-one aligned image pairs, so one can quantitatively evaluate unpaired image-to-image translation models via a distance metric such as mean squared error (MSE) between generated examples and the corresponding ground truth. While MSE can have limitations, it is reasonable for evaluating one-to-one paired datasets. Note that we restrict ourselves to unpaired translation, so the pairing information is omitted during training and only used for evaluation.

Table 2: Mean Squared Error (MSE) comparing CycleGAN and variants of AlignFlow on paired test sets. MSE is computed pixelwise after normalizing images to $(-1, 1)$.

Dataset	Model	MSE (A \rightarrow B)	MSE (B \rightarrow A)
Facades	CycleGAN	0.7129	0.3286
	AlignFlow (Adversarial only)	0.6727	0.2679
	AlignFlow (Hybrid)	0.5801	0.2512
	AlignFlow (MLE only)	0.9014	0.5960
Maps	CycleGAN	0.0245	0.0953
	AlignFlow (Adversarial only)	0.0385	0.1123
	AlignFlow (Hybrid)	0.0209	0.0897
	AlignFlow (MLE only)	0.0452	0.1746
CityScapes	CycleGAN	0.1252	0.1200
	AlignFlow (Adversarial only)	0.2569	0.2196
	AlignFlow (Hybrid)	0.1130	0.1462
	AlignFlow (MLE only)	0.2526	0.2272

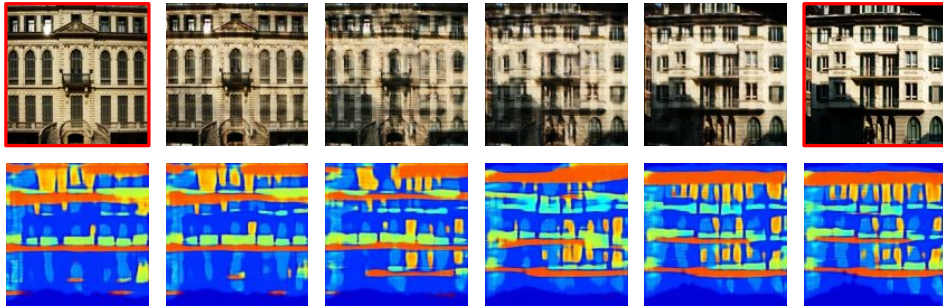


Figure 5: Latent space interpolation on Facades. **Top:** Left-most and right-most images are sampled from \mathcal{D}_A (in red boxes). Interpolation is then performed in latent space and then decoded using $G_{Z \rightarrow A}$. We see semantically meaningful changes across the row, *e.g.*, in the shadow and the style of entrance to the building. **Bottom:** For each corresponding image in the top row, its latent representation is decoded into the target domain using $G_{Z \rightarrow B}$. Inspection of the orange regions indicates a change from 3 floors (left) to 4 floors (right).

We report the MSE for translations on the test sets after cross-validation of hyperparameters in Table 2, leaving the exploration of other perceptual evaluation metrics for future work. For hybrid models, we set $\lambda_A = \lambda_B$. We observe that while learning AlignFlow via adversarial training or MLE alone is not as competitive as CycleGAN, hybrid training of AlignFlow significantly outperforms CycleGAN in almost all cases. Specifically, we observe that MLE alone typically performs worse than adversarial training, but together both these objectives seem to have a regularizing effect on each other.

We use the standard training, validation, and test splits for each dataset. For datasets which do not provide a validation set (*e.g.*, Facades and CityScapes), we randomly hold out a portion of the training set with the same number of images as the test set. We train each model for 200 epochs with a fixed learning rate of $2 \cdot 10^{-4}$ for the first 100 epochs, followed by a linear decay schedule for 100 epochs from the initial learning rate to 0. We use the Adam [60] optimizer with $\beta_1 = 0.5$ and $\beta_2 = 0.999$, and for AlignFlow we apply weight normalization [61] of $5 \cdot 10^{-5}$ to the generator’s parameters. When training with an MLE objective, we apply gradient clipping with a maximum gradient norm of 10. Scaling flow models to higher dimensionality is an active area of research; for this work we resized the images to 64×64 for Cityscapes and Maps, and 128×128 for Facades. We use a batch-size of 16 images.



Figure 6: Examples of failure modes for CycleGAN reconstructions in MNIST \leftrightarrow SVHN cross-domain translation. In each group of 3, a real example is shown on the left, the translated image is shown at center, and the reconstructed image is shown on the right.

For MLE/Hybrid models, we used an isotropic Gaussian prior. We use the following flow architecture to parameterize $G_{Z\rightarrow A}$ and $G_{Z\rightarrow B}$:

```

Scale[Input: 32x32x3, Output: 16x16x6x2]
  → 3x CheckerboardCoupling[Channels: 32, Blocks: 4]
  → 3x ChannelwiseCoupling[Channels: 64, Blocks: 4]
  → Squeeze&Split[Input: 32x32x3, Output: 16x16x6x2]
Scale[Input: 16x16x6, Output: 8x8x12x2]
  → 3x CheckerboardCoupling[Channels: 64, Blocks: 4]
  → 3x ChannelwiseCoupling[Channels: 128, Blocks: 4]
  → Squeeze&Split[Input: 16x16x6, Output: 8x8x12x2]
Scale[Input: 8x8x12, Output: 4x4x24x2]
  → 3x CheckerboardCoupling[Channels: 128, Blocks: 4]
  → 3x ChannelwiseCoupling[Channels: 256, Blocks: 4]
  → Squeeze&Split[Input: 8x8x12, Output: 4x4x24x2]
Scale[Input: 4x4x24, Output: 4x4x24]
  → 4x CheckerboardCoupling[Channels: 256, Blocks: 4]

```

where CheckerboardCoupling and ChannelwiseCoupling are affine coupling layers with checkerboard and channelwise masking, respectively, and where Squeeze&Split first trades spatial extent for channels by turning each $4 \times 4 \times 1$ subvolume into a $1 \times 1 \times 4$ subvolume, and then splits the volume along the last dimension and sends half of the features directly to the latent space. See Dinh et al. [17] for more details. Within each affine coupling layer, we parametrize the scale and translate factors using a ResNet [62] architecture with the specified number of channels and residual blocks. We additionally use activation normalization [32] before each coupling layer.

Latent space interpolations for the Facades dataset are shown in Figure 5. Again, we see that many aspects of style and content are preserved in the samples corresponding to the latent space interpolations.

B.3 Unsupervised Domain Adaptation

One such model relevant to this experiment is Cycle-Consistent Domain Adaptation (CyCADA) [3]. CyCADA first learns a cross-domain translation mapping from source to target domain via CycleGAN. This mapping is used to stylize the source dataset into the target domain, which is then subject to additional feature-level and semantic consistency losses for learning the target domain classifier [34, 63]. A full description of CyCADA is beyond the scope of discussion of this work; we direct the reader to Hoffman et al. [3] for further details.

We use the same training, validation and test splits of MNIST, USPS, and SVHN digit datasets as in CyCADA [3]. For all datasets, images are resized to 32×32 as in CyCADA. We employ the pixel-level and feature-level adaptation training pipeline as in CyCADA but replace the CycleGAN-based image translation network with the AlignFlow. The architectures for imposing semantic consistency and feature adaptation are the same as the ones used for CyCADA. The architecture and hyperparameter tuning protocol was consistent with the one used for image-to-image translations using AlignFlow.

For the hyperparameters of feature-level domain adaptation post the image translations, we adopted the optimal hyperparameter settings from ADDA [34].

Failure Modes of Approximate Cycle Consistency. To show the importance of exact cycle-consistency for domain adaptation, we present a few failure modes in the context of Cycada [3]. In Figure 6, we consider some cross-domain translation cases between MNIST and SVHN. In each group of 3, a real example is shown on the left, the translated image is shown at center, and the reconstructed image is shown on the right. Notice that the class label changes or becomes unrecognizable in translating and reconstructing the input. AlignFlow does not have these failure modes because cycle-consistency is ensured by design and hence, the reverse translations will exactly match the original image in the source domain preserving essential properties like class identity.